https://doi.org/10.5194/egusphere-2023-2256
Preprint. Discussion started: 9 October 2023

Mechanisms of Global Ocean Ventilation Age Change during the Last Deglaciation

Lingwei Li[1], Zhengyu Liu[1], Jinbo Du[2], Lingfeng Wan[3], Jiuyou Lu[4]

[1]Department of Geography, The Ohio State University, Columbus, Ohio, 43210, United States
[2]Department of Atmospheric and oceanic sciences, Peking University, Peking, China
[3]Frontier Science Center for Deep Ocean Multispheres and Earth System (FDOMES) and Physical Oceanography Laboratory, Ocean University of China, Qingdao, China
[4]Laoshan Laboratory, Qingdao, postal code, China

Correspondence to: Lingwei Li (li.8955@osu.edu)

Abstract. Marine radiocarbon (^{14}C) is widely used to trace deep ocean circulation, providing insight into the atmosphere-ocean exchange of CO2 during the last deglaciation. Using two transient simulations with tracers of ^{14}C and ideal age, we found that the oldest ventilation age is not observed at the Last Glacial Maximum (LGM). In contrast, the model shows a modestly younger ventilation age during the LGM compared to present day, mainly due to a stronger glacial Antarctic Bottom Water (AABW) transport associated with sea ice expansion. Notably, the ocean ventilation age is significantly older around 14-12 ka compared to the age at the LGM, with deep Pacific waters playing a predominant role, primarily caused by the weakening of AABW transport.

https://doi.org/10.5194/egusphere-2023-2256
Preprint. Discussion started: 9 October 2023

1 Introduction

Ice core records demonstrate significant variability in atmospheric carbon dioxide (CO_2) concentrations on the glacial-interglacial timescale (Sigman & Boyle, 2000). During the last glacial period, atmospheric CO_2 levels were approximately 90 parts per million by volume (ppmv) lower than the Holocene value of 280 ppmv (11.7-0 ka where ka indicates "thousand years ago") (Monnin et al., 2001; Schmitt et al., 2012). Since the ocean serves as the primary carbon reservoir and its capacity to sequester CO_2 is strongly influenced by global ventilation rates, most proposed mechanisms for this CO_2 reduction involve changes in deep ocean circulation (Sigman et al., 2010; Sigman & Boyle, 2000; Toggweiler, 1999).

Various proxy reconstructions have been used to investigate past changes in oceanic circulation. Notably, radiocarbon ($\Delta^{14}C$) observations are valuable for determining the ventilation age of the ocean, which represents the time elapsed since water last interacted with the atmosphere. Evidence indicates that during the Last Glacial Maximum (LGM; 23-18 ka), the North Atlantic and North Pacific exhibited significant depletion in $\Delta^{14}C$ below approximately 2.5 km compared to present day levels (Marchitto et al., 2007; Rafter et al., 2022; Skinner et al., 2015, 2017). A comparison with other radiocarbon data from the southern high-latitudes suggests consistent changes experienced across the Southern Ocean (Burke & Robinson, 2012; Chen et al., 2015; Schmitt et al., 2012; Skinner et al., 2010). This $\Delta^{14}C$ depletion has been suggested as an indication that the deep waters were isolated and poorly ventilated, leading to an increased ventilation age at the LGM relative to the present day.

The relationship between the $\Delta^{14}C$ depletion at the LGM and the true ocean ventilation time, however, has remained uncertain. Traditionally, two ages can be estimated from the ocean $\Delta^{14}C$ at depth: the $\Delta^{14}C$ B-A age that is estimated from the benthic-atmosphere $\Delta^{14}C$ age difference, and the $\Delta^{14}C$ B-P age that is estimated from the benthic-planktonic $\Delta^{14}C$ age difference, with the difference between the two ages caused by the surface water, or the marine reservoir age. The temporal evolution of the atmospheric $\Delta^{14}C$ during the deglaciation further lead to a changing source of ocean water $\Delta^{14}C$, which leads to the so called projection age (Adkins & Boyle, 1997). An analysis of $\Delta^{14}C$ B-P age in the deep Pacific suggests that ventilation age increased by ~1000 years during the deglaciation, contradicting the expected pattern of an isolated carbon reservoir in the glacial deep North Pacific (Lund et al., 2011). Climate models with radiocarbon have also been used to study ocean ventilation age during the deglaciation. Model simulation shows that sea ice expansion at the LGM contributes to a depletion of ocean $\Delta^{14}C$ and in turn an older radiocarbon age than the true ventilation age (Schmittner, 2003). Recently, Zanowski et al., (2022) assessed the relationship between the evolution of $\Delta^{14}C$ and circulation changes in the deep Pacific Ocean in a transient ocean simulation forced by realistic climate forcing during the last deglaciation (22–0 ka): the C-iTRACE ocean model simulation (Gu et al., 2019, 2020, 2021). They found that the deglacial variations in Pacific Ocean $\Delta^{14}C$ age are influenced by changes in both the deep circulation and surface ocean reservoir age. Therefore, the $\Delta^{14}C$ age could differ substantially from the true ocean ventilation age.

https://doi.org/10.5194/egusphere-2023-2256
Preprint. Discussion started: 9 October 2023

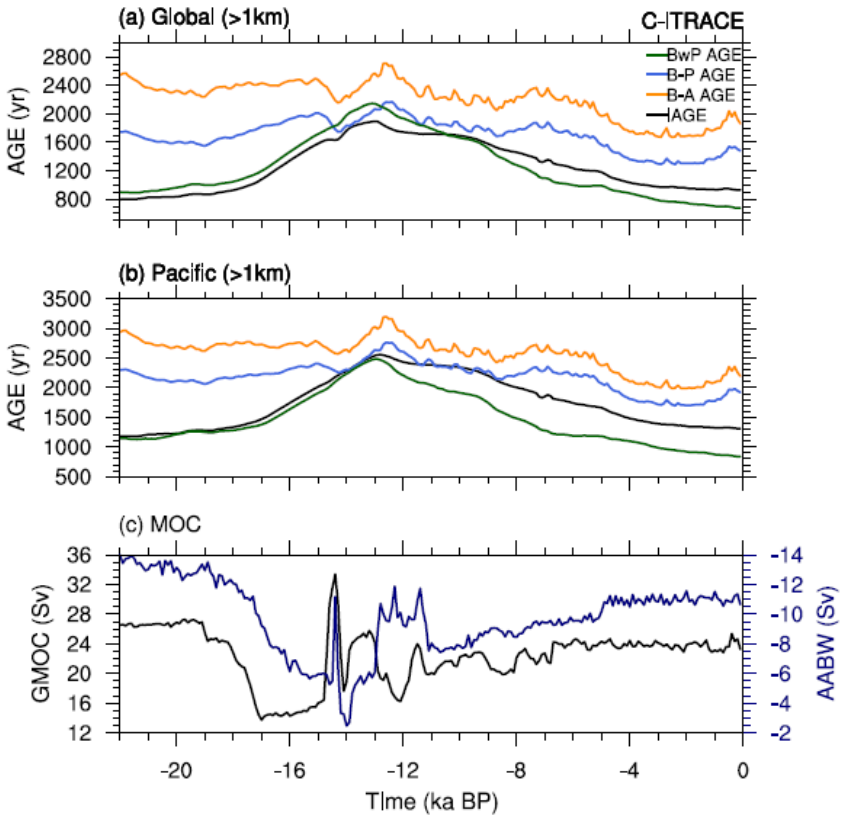

Figure 1 Time evolutions in the C-iTRACE: (a) The global mean ideal age (IAGE; black), benthic-atmosphere Δ^{14}C age (B-A age; yellow), benthic-planktonic Δ^{14}C age (B-P age; blue), and weighted benthic-planktonic Δ^{14}C age (BwP age; green) averaged below 1 km. (b) The Pacific mean IAGE (black), B-A age (yellow), B-P age (blue), and BwP age (green) averaged below 1 km. (c) The Global Meridional Overturning Streamfunction (GMOC; black) and Antarctic Bottom Water strength (AABW; navy). Here GMOC is defined as the maximum magnitude of transport in GMOC from 33° S-60° N between 0.6 – 3.5 km, and AABW is defined as the minimum magnitude of transport in GMOC from 2° S-70° S below 2 km.

In this study, we examine the global ocean ventilation time in the C-iTRACE simulation. Figure 1a shows the deglacial evolutions of the B-A age and B-P age averaged globally below 1 km. The B-A age is calculated as $8267 \times ln(\frac{\frac{\Delta^{14}C_{atmosphere}}{1000}+1}{\frac{\Delta^{14}C_{ocean}}{1000}+1})$, where $\Delta^{14}C_{atmosphere}$ is the Δ^{14}C in the atmosphere, and the B-P age is calculated as $8267 \times ln(\frac{\frac{\Delta^{14}C_{surface}}{1000}+1}{\frac{\Delta^{14}C_{ocean}}{1000}+1})$, where $\Delta^{14}C_{surface}$ is the Δ^{14}C average value of upper 100 m of the ocean. These two ages are compared with the true global ocean ventilation age in the model, or the ideal age (IAGE). First, both the B-A age and B-P age are remarkably old at the LGM (~20 ka) than the present day (PD, ~0 ka), and show decreasing trend from the LGM towards the PD. This is largely consistent with the observations of more depleted deep water Δ^{14}C at the LGM (Burke & Robinson, 2012; Chen et al., 2015; Okazaki et al., 2010; Rafter et al., 2022; Skinner et al., 2017, 2019). Second, both the B-A age and

https://doi.org/10.5194/egusphere-2023-2256
Preprint. Discussion started: 9 October 2023

B-P age are significantly older than the IAGE, with dramatically different deglacial evolution pattern. The IAGE is slightly younger at the LGM than at the present and ages dramatically by over two times towards before the Younger Dryas (YD; 12.9-11.7 ka), in sharp contrast to the radiocarbon ventilation ages that showed minimal change before the YD and then a predominately decreasing trend in the Holocene. Similar behaviors of the radiocarbon ages and IAGE are also present in the Pacific Ocean (Figure 1b). These radiocarbon ages raise two questions in the model context. First, why are the radiocarbon ages different from the true ventilation age, and how to estimate the true ocean ventilation age from the ocean radiocarbon? Second, why is the true ocean ventilation age comparable between the LGM and the present, and why does it increase to its oldest age before the YD?

The first question will be discussed in a separate paper (Du et al., in prep), which proposes a new method to estimate the ventilation age from radiocarbon using the so called weighted benthic-planktonic $\Delta^{14}C$ age (BwP age) by taking account of multiple water mass contributions (Fig. 1a and 1b green lines). This new approach of BwP age is incredibly identical to the true ocean ventilation age globally, suggesting that water age is not old at the LGM and, instead, peak in the middle of deglaciation around 13 ka. The similar temporal evolution patterns of BwP age and model ventilation age suggest that B-P and B-A ages are likely biased by remote water mass sources (e.g. Antarctic Bottom Water from the Southern Ocean) and can be greatly improved. Since the existing proxies have not been able to provide a comprehensive understanding on the true ocean ventilation deglacial evolution, we will address the second question on the mechanism of the deglacial evolution of the model ventilation time, in order to provide some constraints on the global ocean ventilation age changes during the last deglaciation.

In this study, we show that the deep ocean ventilation time in the model is determined mainly by the circulation of the Antarctic Bottom Water (AABW) with the deep Pacific playing the dominant role. We will describe the model simulation and method in section 2. The mechanism of the evolution of the ocean ventilation time is discussed in detail for C-iTRACE in section 3 and briefly for another simulation iTRACE in section 4. A summary is given in section 4.

2 Models and data

We will analyze the C-iTRACE simulation, which is an ocean-only deglacial transient simulation (22 – 0 ka) in the isotope-enabled version of the Parallel Ocean Program version 2 (POP2; Danabasoglu et al., 2012), the ocean component of the Community Earth System Model (CESM). The model configuration comprises 60 vertical layers and a nominal 3° horizontal resolution. The C-iTRACE is forced by the monthly surface forcings (heat flux, freshwater flux, and momentum flux) from a fully coupled transient simulation (TRACE-21ka), which is forced by realistic external forcing of continental ice sheet, greenhouse gases, orbital forcing, and melting water fluxes and simulates many key features of the last deglaciation (Liu et al., 2009). The simulation incorporates multiple geotracers, such as carbon isotopes (Jahn et al., 2015), neodymium isotopes (Gu, Liu, Jahn, et al., 2019), $^{231}Pa/^{230}Th$ ratio (Gu & Liu, 2017), and oxygen isotopes (Zhang et al., 2017). The incorporation of geotracers in the C-iTRACE facilitates a direct model-data comparison, and the transient simulation C-iTRACE has been

https://doi.org/10.5194/egusphere-2023-2256
Preprint. Discussion started: 9 October 2023

used in many recent studies to understand intermediate and deep water masses and oceanic circulation variations (Gu et al., 2020; Gu, Liu, Oppo, et al., 2021; Zanowski et al., 2022; Zhang et al., 2017).

To further improve the understanding of deglacial deep ocean ventilation changes and associated mechanisms, several idealized tracers are also implemented in C-iTRACE. First, the ideal age (IAGE) is included, which is set to 0 at the ocean surface and ages at a rate of 1 year/year thereafter passively advected and diffused into the ocean interior. Thus, IAGE represents the true model ventilation age, but it does not account for the insulation effect of sea ice. Second, several dye tracers are implemented in the model to identify water mass composition. The dye tracers are reset to 1 over specific region at the ocean surface during each time step and passively advected and diffused within the ocean interior. In this study, two dye tracers are used over the surface Southern Ocean (south of 34°S, Dye_S) and the North Atlantic (north of 40°N, Dye_NA). Detailed descriptions of these tracer experiments can be found in previous manuscripts (Gu et al., 2020, 2021; Zanowski et al., 2022).

In addition to C-iTRACE, we also analyze the deglacial ventilation age changes in another fully-coupled deglacial simulation, iTRACE, conducted with the isotope-enabled CESM (iCESM, Brady et al., 2019). The iTRACE experiments are performed following a similar strategy as in the previous transient simulation TRACE-21ka (Liu et al., 2009), but in the state-of-the-science CESM1.3 (Hurrell et al., 2013). Similar to C-iTRACE, the ocean component of iTRACE consists of 60 vertical layers, but with a higher nominal 1° horizontal resolution. It also includes multiple geotracers, such as radiocarbon, oxygen isotopes, and IAGE, although, unfortunately, the radiocarbon output is only available from 20 ka to 11 ka in this paper. The iTRACE has been directly compared to multiple proxy reconstructions and is able to quantitatively capture many major features of climate variations during the last deglaciation (Brady et al., 2019; Hurrell et al., 2013). Further details regarding the iTRACE simulation can be found in previous manuscripts (He et al., 2021a, 2021b).

In the following analyses, the time resolution for all variables is 100-year average in both simulations, and all times (calendar ages) are reported in thousands of years before present (ka BP). Climatologies for the LGM and PD states in the C-iTRACE are taken as the 100 year means of 20 ka and 0 ka respectively.

3 C-iTRACE results

3.1 LGM and PD ventilation ages

Our model shows a modestly younger ventilation age (IAGE) in the deep ocean at the LGM compared to the PD. Specifically, at depths below 1 km, the global mean IAGE is 800 years at the LGM, whereas it is 930 years at the PD (Fig. 1a). Similarly, for the Pacific region, the IAGE is 1181 years at the LGM, in contrast to 1310 years at the PD (Fig. 1b). This modestly younger LGM IAGE can also be seen in comparison of the global zonal mean between the LGM and PD (Fig. 2a and 2c). The maximum IAGE in the deep ocean is 1660 years during the LGM and 1763 years during the PD. Therefore, it suggests that the deep ocean is not poorly ventilated with older ventilation age at the LGM than today in the model.

https://doi.org/10.5194/egusphere-2023-2256
Preprint. Discussion started: 9 October 2023

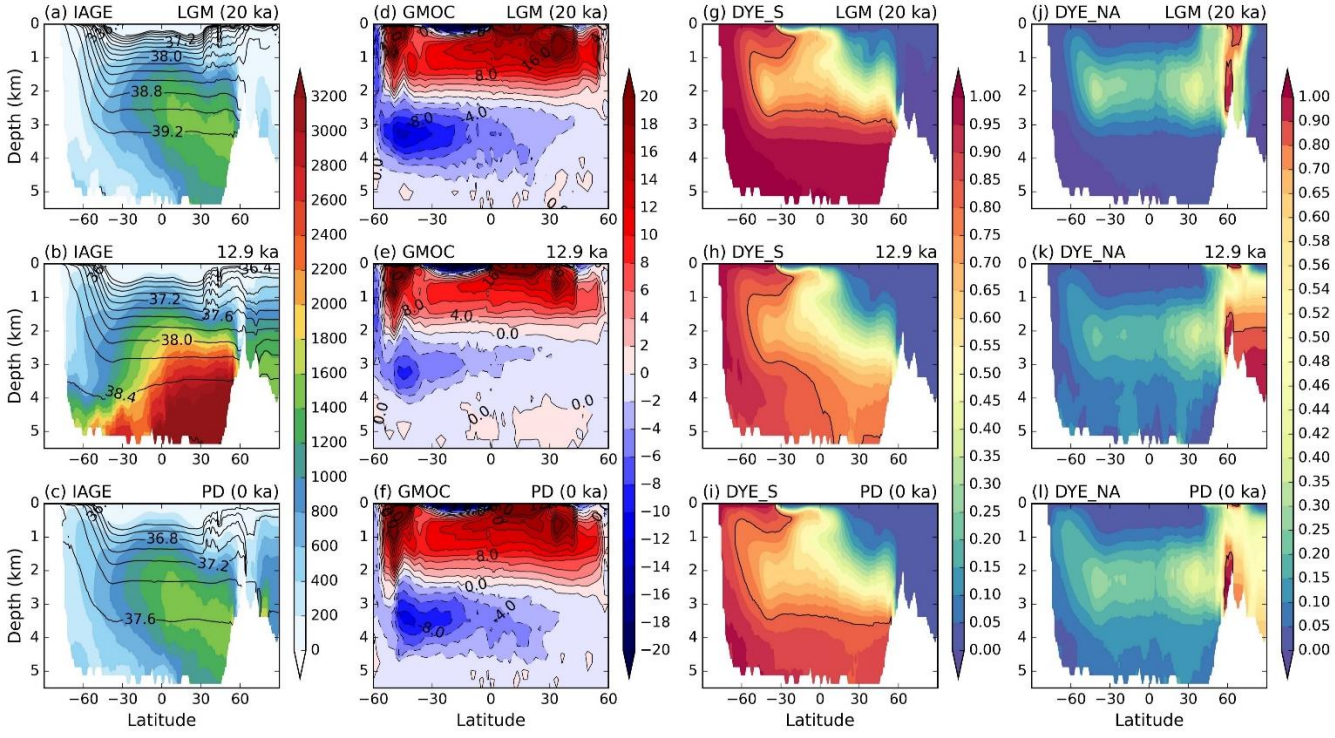

Figure 2 The global zonal mean distributions at LGM (20 ka), 12.9 ka, and present day (PD, 0 ka). (a-c) IAGE (shading; unit in year) with isopycnals (σ2; potential density referenced to 2000 m; black contour lines; unit in kg/m^3). (d-f) Global residual meridional overturning circulation (GMOC; unit in Sv). (g-i) Dye-South: water originating from the Southern Ocean. (j-l) Dye-North: water originating from the North Atlantic. The thick black contours on dye tracers (g-l) represent the value of 0.8. Note the nonlinear magnitude of the colour bar for Dye-North.

To elucidate the reasons behind the younger LGM IAGE, we first explore whether it is likely attributed to the AABW transport. The deep ocean circulation generally consists of two cells (Marshall & Speer, 2012; Talley, 2013). The first cell, known as the upper cell, starts with the deep water North Atlantic Deep Water (NADW) formation. The NADW source water sinks into deeper depth at the northern Atlantic and then flows southward at middepth in the basin primarily along deep western boundary all the way to the Southern Ocean before upwelling along isopycnals and eventually flowing back northward as intermediate waters. The second cell, known as the abyssal cell, starts with the bottom water AABW formation in the Southern Ocean. The AABW water mass sinks into the abyss from its formation sites around the Antarctica and moves northward across topography to fill the deepest parts of the global ocean. It then upwells to middepth before returning to the surface along isopycnals in the Southern Ocean. Because AABW occupies the largest volume of any water mass in the ocean, driving the lower limb of the global overturning circulation (Johnson, 2008; Talley, 2013), it is reasonable to hypothesize that a reduction in AABW volume transport is linked to a decrease in abyssal ocean ventilation rate and, in turn, an increase of ventilation time. This hypothesis is supported by the C-iTRACE analysis. Here, the maximum magnitude in the abyssal global residual Meridional Overturning Circulation (GMOC) is 13.1 Sv (1 Sv ≡ 10^6 m^3 s^{-1}) at the LGM and 10.6

https://doi.org/10.5194/egusphere-2023-2256
Preprint. Discussion started: 9 October 2023

Sv at the PD (Fig. 2d and 2f). The intensified LGM AABW transport in the C-iTRACE is consistent with some reconstructions and modelling studies showing larger salinification of AABW, such that glacial deep ocean is filled with cold-salty AABW water mass and higher densities lead to a stronger AABW transport (Adkins et al., 2002; Hesse et al., 2011; Negre et al., 2010; Schmittner, 2003). Model simulations further indicate that the strong glacial AABW transport can be attributed to changes in surface buoyancy forcing and deep ocean stratification associated with sea ice expansion in the Southern Ocean (Ferrari et al., 2014; Jansen, 2017; Jansen & Nadeau, 2016; Shin et al., 2003; Sun et al., 2018). Thus, it implies that the depleted deep water $\Delta^{14}C$ at the LGM is more likely linked to reservoir age, instead of a slower overturing circulation (Skinner et al., 2017, 2019). Here, it suggests that the IAGE exhibits an overall younger ventilation age at the LGM than the PD, primarily contributed by the stronger AABW transport.

The dominant role of the AABW transport in determining the ventilation age at the LGM is also evident in the idealized dye concentrations. Since the water mass distributions can be identified unambiguously using dye tracers, the comparison between the IAGE and dye tracers shows the younger LGM IAGE is likely associated with vigorous AABW. Below 3 km, the average proportion of AABW (AABW%) represented by dye concentration from the Southern Ocean (Dye_S) is 86% at the LGM (Fig. 2g), which is 16% higher than that observed at the PD (Fig. 2i). This high AABW% coincides with the strong northward AABW flow (Fig. 2d) and the notable young ventilation age in the deep ocean at the LGM (Fig. 2a). In contrast, the fraction of NADW (NADW%), indicated by dye concentration from the North Atlantic (Dye_NA), remains relatively low at 2% and 18% below 3 km during the LGM and PD, respectively, except in the Arctic Ocean (Fig. 2j and 2l). Thus, the fractions of NADW and AABW illustrate the dominant role of AABW, in comparison to NADW, in filling the abyssal ocean and influencing deep ocean ventilation age.

The dominant role of AABW in deep ventilation age at the LGM can be further quantified by calculating the deep ventilation age of the AABW and NADW water masses. We calculate the IAGE value where the percentages of AABW% and NADW% exceed 70% below 1 km in the global ocean (Fig. 3a). The averaged IAGE for AABW is about 833 years at the LGM and 921 years at the PD, while the IAGE for NADW is about 200 years at both the LGM and PD. Furthermore, the volume of AABW is about $8\ 10^8$ km^3 at the LGM and PD, such that the volume integrated IAGE for AABW is about $7\ 10^{11}$ yr km^3 at both LGM and PD (Fig. 3b and 3c). Thus, the younger ventilation age in the deep ocean at the LGM is caused by a relatively younger AABW at the LGM than the PD.

https://doi.org/10.5194/egusphere-2023-2256
Preprint. Discussion started: 9 October 2023

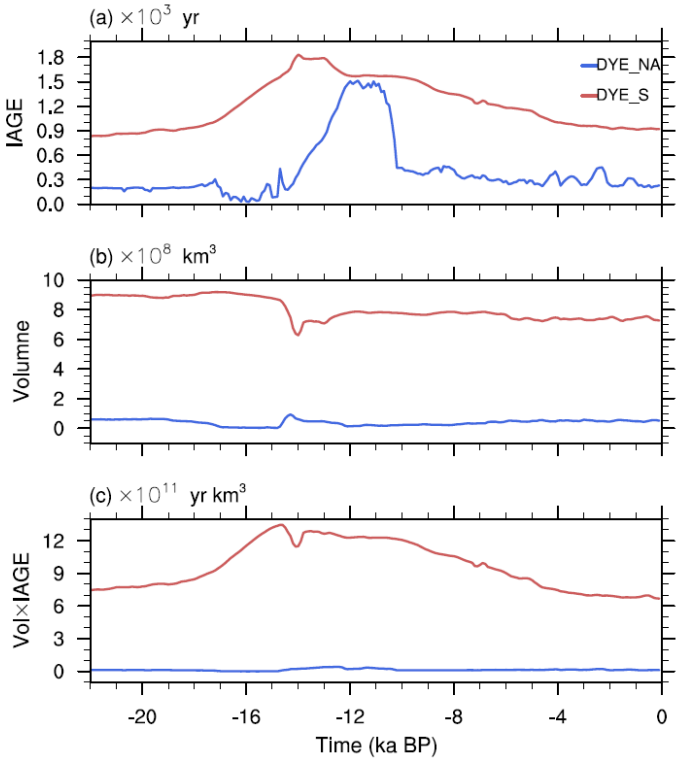

Figure 3 Time evolutions for water masses sourced from different regions. (a) The global volume-weighted average of ideal age (IAGE) where fractions of water originating from the Southern Ocean (red) and North Atlantic (blue) are greater than 70%. (b) The total water volume where fractions of water originating from the Southern Ocean (red) and North Atlantic (blue) are greater than 70%. (c) The age of total volume of water from the Southern Ocean and North Atlantic (the product of volume from (b) and the global averaged ideal age from (a)).

3.2 Mechanisms for deglacial evolution of ventilation age

In comparison with the almost comparable IAGEs of LGM and PD, the deglacial evolution exhibits a dramatic bell shape, with the global deep IAGE increasing from 800 years at the LGM to its oldest value of more than doubled to 1900 years at 12.9 ka, followed by a decline back towards 930 years in the Holocene period (Fig. 1a). A similar bell shape pattern is also seen for the Pacific mean (Fig. 1b). This dramatically older deep water at 12.9 ka is also seen clearly in comparison of the oldest water in the global zonal mean IAGE, which is 3847 years at 12.9 ka, more than doubling the oldest ages of 1660 years at the LGM and 1763 years at the PD (Fig. 2a-c). This deglacial evolution of global IAGE can be also seen in the depth-time Hovmöller diagram of global IAGE (Fig. 4a). Across the depth, the ventilation age is relatively younger at the LGM in the deep ocean, and there is a middepth maximum in water ages mainly because of strong AABW as discussed in section 3.1. More importantly, the IAGE tends to increase monotonically from the LGM to Heinrich Stadial 1 (HS1; 17.5-14.7 ka), reaching to its oldest value in the deep ocean around 12.9 ka, and subsequently becoming younger toward the PD.

https://doi.org/10.5194/egusphere-2023-2256
Preprint. Discussion started: 9 October 2023

This bell shaped deglacial evolution of global IAGE aligns with a similar transport evolution of the abyssal GMOC and AABW (Fig. 1c, Fig. 2d-f) as well as the AABW% in dye tracers from the Southern Ocean (Fig. 3, Fig. 2g-i). A more careful observation shows that the evolution of IAGE is more similar to the strength of AABW than GMOC, as exhibited by the decrease in AABW transport and the increase in IAGE during the same period (14–13 ka). Therefore, this evolution appears still consistent with the hypothesis that the deep ventilation time is controlled mainly by the AABW transport during the deglaciation.

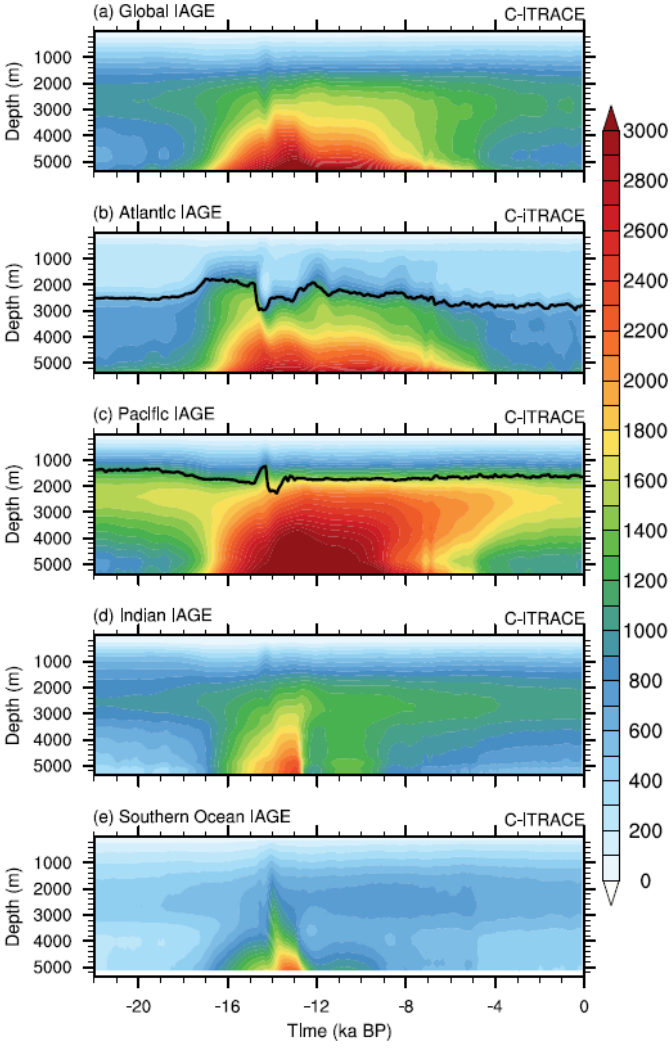

Figure 4 Depth-time Hovmöller diagram of IAGE averaged over global and different basins. (a) The global mean. (b) Atlantic basin average. (c) Pacific basin average. (d) Indian basin average. (e) Southern Ocean average. The thick black lines on (b) and (c) are the depth of the zero-contour of Atlantic and Pacific Meridional Overturning Streamfunction averaged between 60° N and 30° S respectively.

https://doi.org/10.5194/egusphere-2023-2256
Preprint. Discussion started: 9 October 2023

To further understand how the AABW variation changes deep ventilation time during the deglaciation, we analyze the ventilation age and AABW transport across different ocean basins. The time evolutions of IAGE in each basins show similar bell-shaped patterns, with the ventilation age increasing in the deep ocean during deglaciation, towards its maximum at 14.5 ka in the Atlantic and 12.9 ka in the Pacific, and then decreasing towards the Holocene (Fig. 4b-e). Relatively, the oldest water always occurs in the deep Pacific, about 700 years older than the deep Atlantic with the largest volume, suggesting that the Pacific Ocean dominates global ocean ventilation age, harbouring the oldest water mass mixture during the last deglaciation.

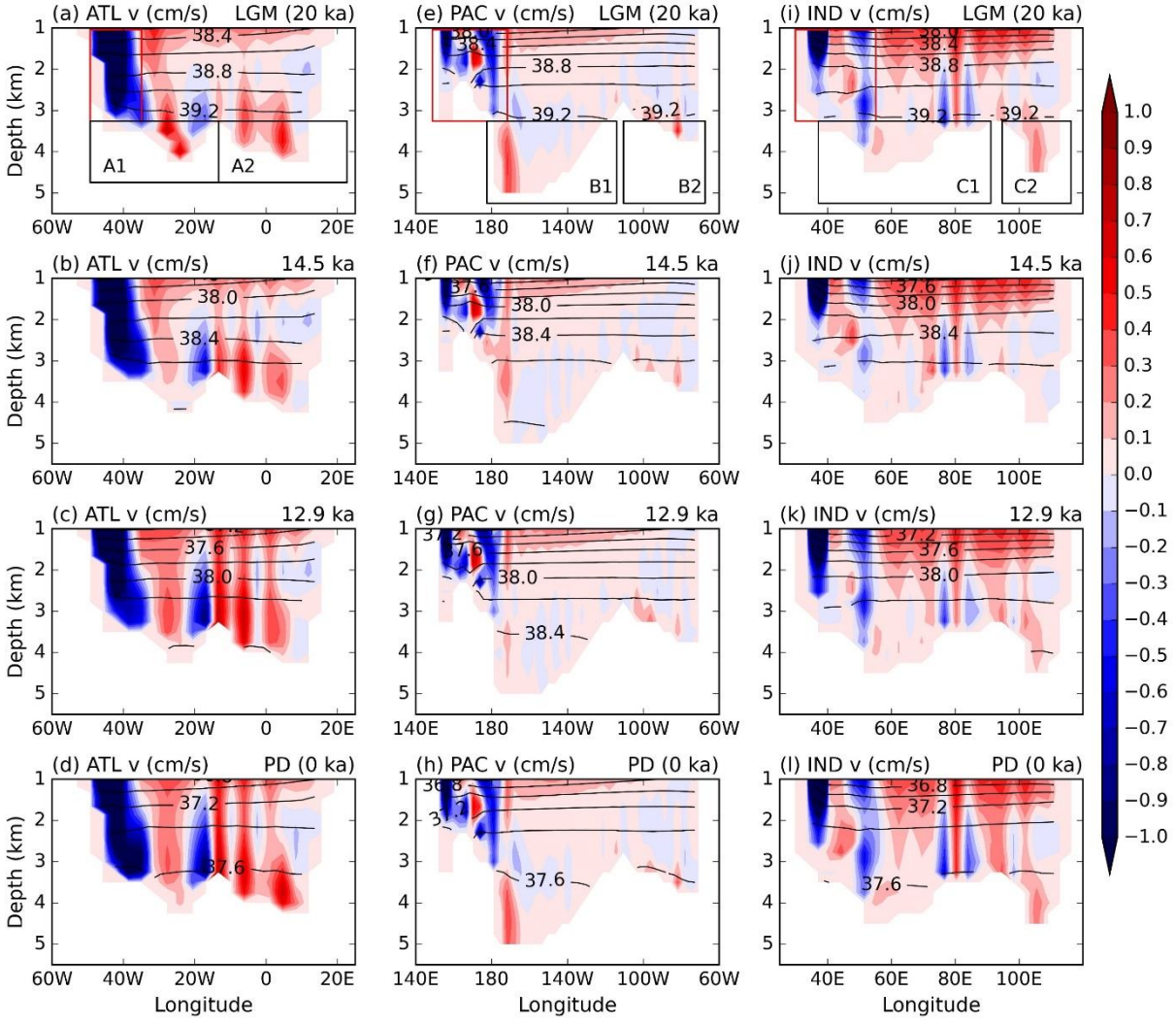

Figure 5 Meridional velocity (shading) and potential density (lines) referenced to 2000 m at 30° S during the LGM (20 ka), 14.5 ka, 12.9 ka, and PD (0 ka) in the C-iTRACE. The shading contour interval is 0.1 cm/s and the black line contour interval is 0.2 kg/m^3. The southward deep western boundary current is defined as the southward integrated volume transport within the highlighted red box on (a, e, i) for the Atlantic, Pacific, and Indian Oceans respectively. The export pathways of AABW in each basin is calculated

https://doi.org/10.5194/egusphere-2023-2256
Preprint. Discussion started: 9 October 2023

as the northward integrated volume transport within the black boxes on (a, e, i), noted as A1 and A2 for the Atlantic, B1 and B2 for the Pacific, and C1 and C2 for Indian Ocean.

We next examine whether the rise in deglacial ventilation age can be explained by the weakening of AABW transport in each basin individually. Along the western boundary of each basin, deep western boundary currents (DWBCs) of northward AABW are observed at different times, notably at the LGM, 14.5 ka, 12.9 ka, and PD, although the currents are strongly diffused by the coarse model resolution (Fig. 5). In the Atlantic below 1 km, the southward DWBC carries the NADW from the subpolar North Atlantic while the northward abyssal DWBC against the continental slope carries the AABW northward, with the AABW DWBC lying beneath and offshore of the NADW DWBC (Fig. 5a-d). In the Pacific and Indian Oceans, only northward DWBCs are present in the abyssal layers, carrying the dense AABW northward (Fig. 5e-l). Moreover, the meridional velocity for bottom AABW flow weakens at 14.5 ka in the Atlantic basin (Fig. 5b), and at 12.9 ka in the Pacific and Indian Oceans (Fig. 5g and 5k), consistent with the IAGE trend shown in Figure 4b and 4c. This supports the bottom AABW current as the primary cause of the deglacial increase in ventilation age.

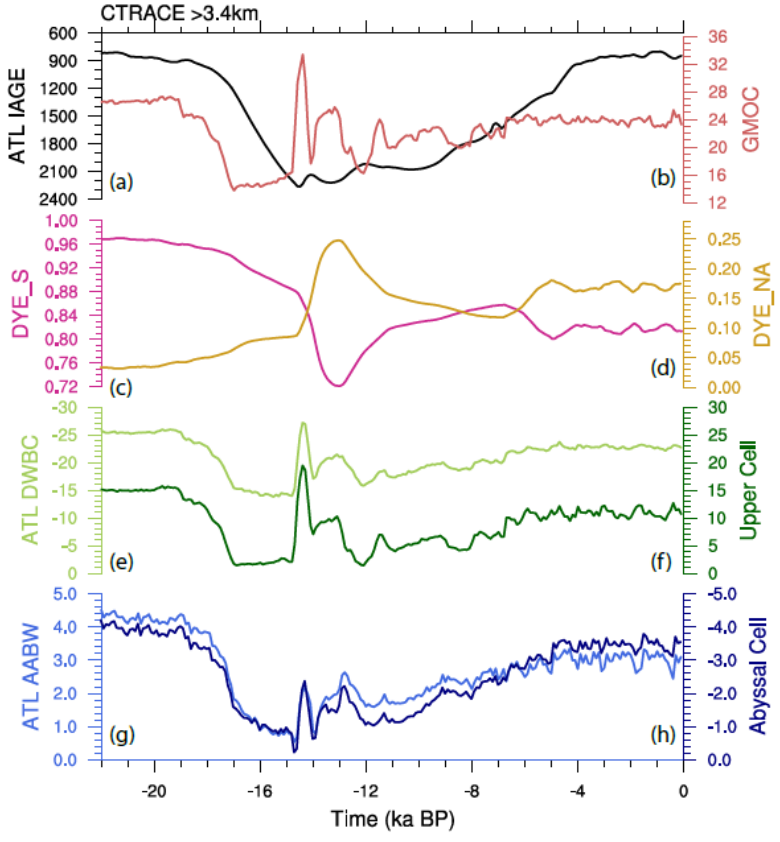

Figure 6 Atlantic deglacial evolutions in the C-iTRACE: (a) IAGE (black) averaged below 3.4 km, (b) GMOC strength (red) defined the same as that in Figure 1c, (c) Dye-South (magenta) averaged below 3.4 km, (d) Dye-North (yellow) averaged below 3.4 km, (e) Southward Deep Western Boundary Current (DWBC; light green) defined as the southward integrated volume transport within the red box in Figure 5, (f) Upper cell (dark green) defined as the maximum in Atlantic Meridional Overturning

https://doi.org/10.5194/egusphere-2023-2256
Preprint. Discussion started: 9 October 2023

Circulation (AMOC) between 0.6-3.5 km at 30° S, (g) AABW transport (light blue) defined as $\Psi_{AABW} = -\int_{z=-H}^{z=-3.4km} \int v\, dxdz$ where v is meridional velocity component and H is the bottom seafloor, and (h) abyssal cell (dark blue) defined as the minimum in AMOC below 2.5 km m at 30° S.

More quantitatively, the AABW transport in each basin will be calculated from the meridional velocity across section at the southern edge 30° S, using the basin wide integrated volume transport below 3.4 km as $\Psi_{AABW} = -\int_{z=-H}^{z=-3.4km} \int v\, dxdz$ where v is meridional velocity component and H is the depth of the seafloor. This is because the isopycnals (potential density referenced to 2000 m) across each basin at 30°S exhibit minimal changes below 3.4 km, and the bottom AABW currents are strongly diffused by the coarse model resolution with very weak interior flow (Fig. 5). The southward DWBC in the deep to intermediate layers is thus defined as the southward integrated volume transport within the red box shown in figure 5a, 5e, and 5i. The estimations of southward DWBC and northward AABW DWBC are confirmed by the model MOCs (Upper and Abyssal cells in the figures). The upper cell is diagnosed as the maximum in the overturning streamfunction between 0.6–3.5 km at 30° S and the abyssal cell is diagnosed as the minimum in the overturning streamfunction below 2.5 km at 30° S. The calculated northward AABW DWBC transport aligns exceptionally well with the transport of model abyssal upper cell in each basin (Fig. 6g-h, Fig. 7g-h). The transports of the southward DWBC and model upper cell are differed by the northward return flow in the interior ocean (Fig. 6e-f, Fig. 7e-f).

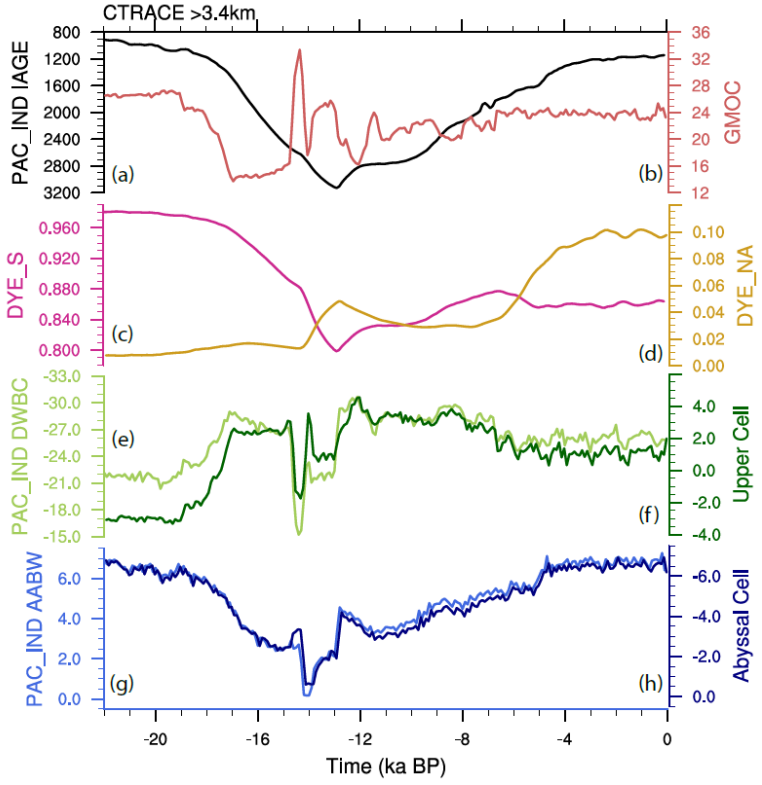

Figure 7 Similar to Fig. 6 but for Indo-Pacific basin.

https://doi.org/10.5194/egusphere-2023-2256
Preprint. Discussion started: 9 October 2023

In the Atlantic basin, the deglacial increase in ventilation age is tied to the reduction of AABW transport. The IAGE averaged across the Atlantic basin below 3.4 km increases from 820 years at the LGM to its oldest age of 2260 years at 14.5 ka, followed by a decrease back towards 840 years at the PD (Fig. 6a). The northward AABW DWBC transport tracks the evolution of IAGE more closely, as AABW transport slows to 0.2 Sv at 14.5 ka and then recovers to 3 Sv at the PD (Fig. 6g). Therefore, the weakening of AABW transport during deglaciation corresponds to a slower ventilation rate and in turn an older ventilation age in the abyssal Atlantic basin.

Transient dye tracer concentrations further support the dominant role of the AABW transport in determining deglacial deep ventilation age. The averaged AABW% declines from LGM to 12.9 ka, indicating a reduced AABW transport flowing into Atlantic (Fig. 6c). In the meantime, the NADW% rises to 25% from LGM to 12.9 ka, contributing to a relatively small portion of younger water flushing the deep Atlantic (Fig. 6d). Note that the ventilation age of AABW water mass is typically much older than the age of NADW (Fig. 3). The mean IAGE for AABW water mass increases from 836 years at the LGM to 1813 years at 14 ka, while the age of NADW increases by up to 1500 years during the period of 12–11 ka due to more NADW sinking into deeper depths in the Arctic, resulting in a relatively older water age for NADW. However, because AABW% in the abyssal Atlantic is substantially higher than NADW% (Fig. 6c and 6d), the presence of the oldest water at 14.5 ka can be mainly attributed to the weakened AABW transport.

The influence of weakened AABW on the deglacial increase in ventilation age is also prominently evident in the Indo-Pacific sector. The IAGE averaged across the Indo-Pacific basin becomes older from the LGM to 12.9 ka, coinciding with the decrease in northward AABW DWBC transport to 2.1 Sv at 12.9 ka (Fig. 7a and 7g). In addition, the AABW% decreases to its minimum value at 12.9 ka, indicating a reduced AABW transport flowing into the Indo-Pacific basin at that time (Fig. 7c). Therefore, the deglacial increase of IAGE in the Indo-Pacific can be mostly explained by the weakening of AABW.

In addition to the AABW transport variations in each basin, the export pathways of AABW from the Southern Ocean into each basin are also explored. Particularly, branches of AABW transport in each basin is calculated as the northward integrated volume transport at 30° S within the black boxes shown in Figure 5a, 5e, and 5i. The deglacial changes of each AABW branch are shown in Figure 8. In the Atlantic at 30° S, the main export route occurs within broad belts east of the Mid Atlantic Ridge (Fig. 8a). The Pacific AABW flows northward along the southwest Pacific basin and is a major source of waters ventilating the deep Pacific basins (Fig 8b). In the Indian Ocean, however, the AABW transport is relatively smaller than that in the Atlantic and Pacific Oceans, and deep pathway of AABW is mainly along the eastern Indian Ocean basin (Fig 8c). The AABW pathways in the Pacific are generally consistent with the available modern observations (Purkey et al., 2018), but different circulation routes of AABW in the Atlantic and Indian Oceans are found in the C-iTRACE, probably due to model deficiencies such as the coarse resolution and eddy-parameterization.

https://doi.org/10.5194/egusphere-2023-2256
Preprint. Discussion started: 9 October 2023

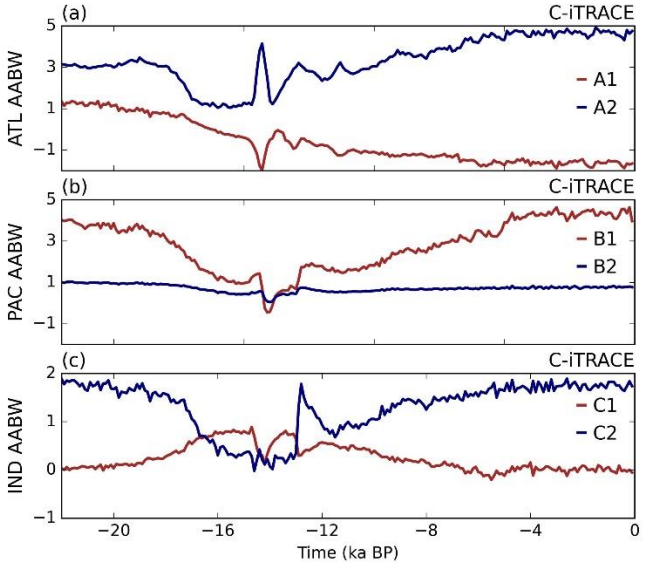

Figure 8 Time evolutions of AABW export pathways into the (a) Atlantic, (b) Pacific, and (c) Indian Oceans in the C-iTRACE. The AABW branch in each basin is calculated as the northward integrated volume transport within the black boxes on Figure 5a, 5e, and 5i, noted as A1 and A2 for the Atlantic, B1 and B2 for the Pacific, and C1 and C2 for Indian Ocean.

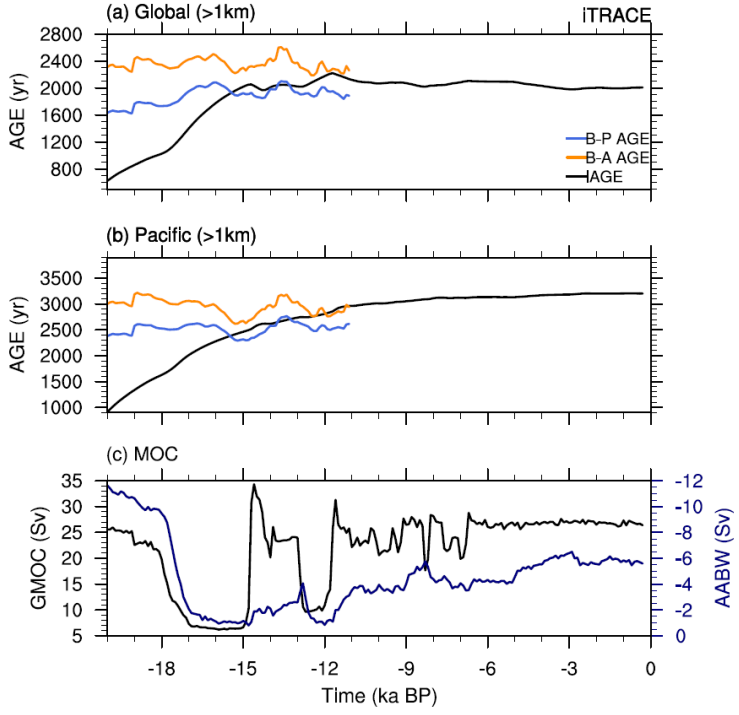

Figure 9 Time evolutions in the iTRACE: (a) The global mean ideal age (IAGE; black), B-A age (yellow), and B-P age (blue) averaged below 1 km. (b) The Pacific mean IAGE (black), B-A age (yellow), and B-P age (blue) averaged below 1 km. (c) The

https://doi.org/10.5194/egusphere-2023-2256
Preprint. Discussion started: 9 October 2023

GMOC (black) and AABW strength (navy). GMOC is defined as the maximum in GMOC from 33° S-60° N between 0.6–3.5 km, and AABW is defined as the maximum in GMOC from 2° S-70° S below 2 km.

4 iTRACE results

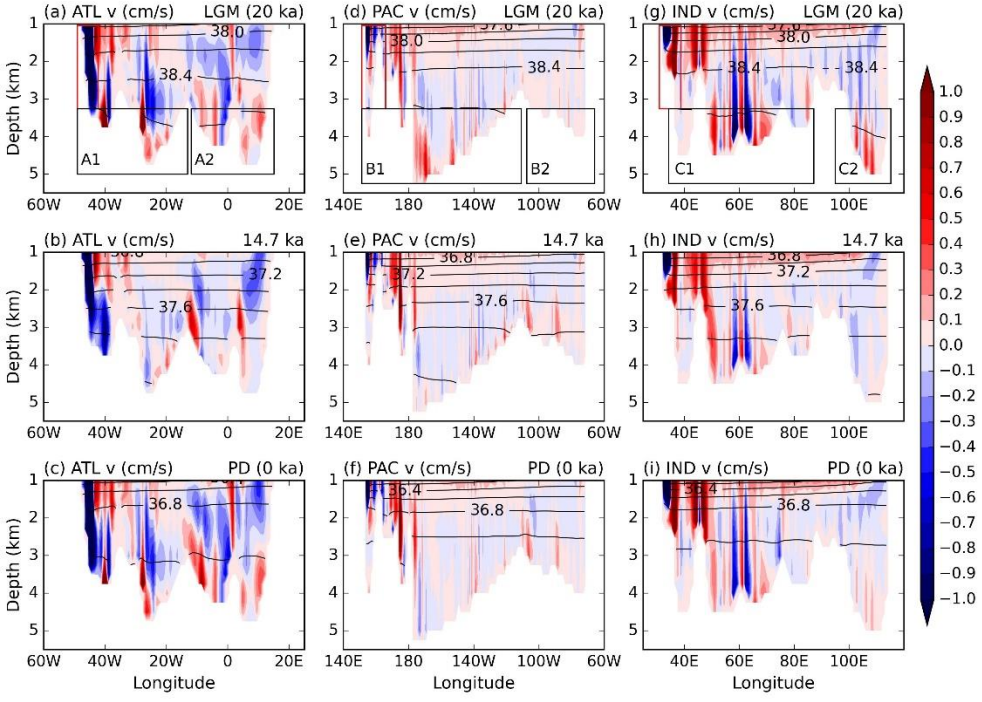

Figure 10 . Meridional velocity (shading) and potential density (lines) referenced to 2000 m at 30° S during the LGM (20 ka), 14.7 ka, and PD (0 ka) in the iTRACE. The shading contour interval is 0.1 cm/s and the black line contour interval is 0.2 kg/m^3. The deep western boundary current excluding AABW is defined as the southward integrated volume transport within the highlighted red box on (a, d, g) for the Atlantic, Pacific, and Indian Oceans respectively. The export pathways of AABW in each basin is calculated as the northward integrated volume transport within the black boxes on (a, d,g), noted as A1 and A2 for the Atlantic, B1 and B2 for the Pacific, and C1 and C2 for Indian Ocean.

In addition to C-iTRACE, we will also explore iTRACE simulation with higher resolution. Results in the iTRACE and C-iTRACE display some similarities. The iTRACE consistently simulates a younger ventilation age at the LGM compared to the PD. The IAGE averaged below 1 km is 626 years and 915 years at the LGM for the global mean and Pacific mean, in contrast to 2011 years and 3203 years at the PD, respectively (Fig. 9a and 9b). The younger LGM IAGE also appears to be linked to the strong AABW in the iTRACE. The maximum magnitude in the abyssal GMOC is 11.6 Sv at the LGM and 5.6 Sv at the PD (Fig. 9c). Hence, the simulation results in both the C-iTRACE and iTRACE point toward a robust younger ventilation age at the LGM than at the PD, both because of the faster overturing rate of AABW relative to the PD.

Moreover, the analysis of the deglacial ventilation age and AABW transport across the different basins in the iTRACE supports results in the C-iTRACE. The IAGE averaged below 3.4 km increases to its maximum of 2460 years at 14.7 ka in

https://doi.org/10.5194/egusphere-2023-2256
Preprint. Discussion started: 9 October 2023

the Atlantic (Fig. 11a), and 3500 years at 6.6 ka in the Indo-Pacific basin (Fig. 12a). The older IAGE in the Pacific suggests that the oldest water always occurs in the deep Pacific dominating the global ocean ventilation age during the last deglaciation. The dominant role of Pacific on deglacial ventilation age appears to be unsurprising as AABW is the sole source of the deep water in the Pacific and Indian oceans, with much less direct input from NADW (Talley, 2013).

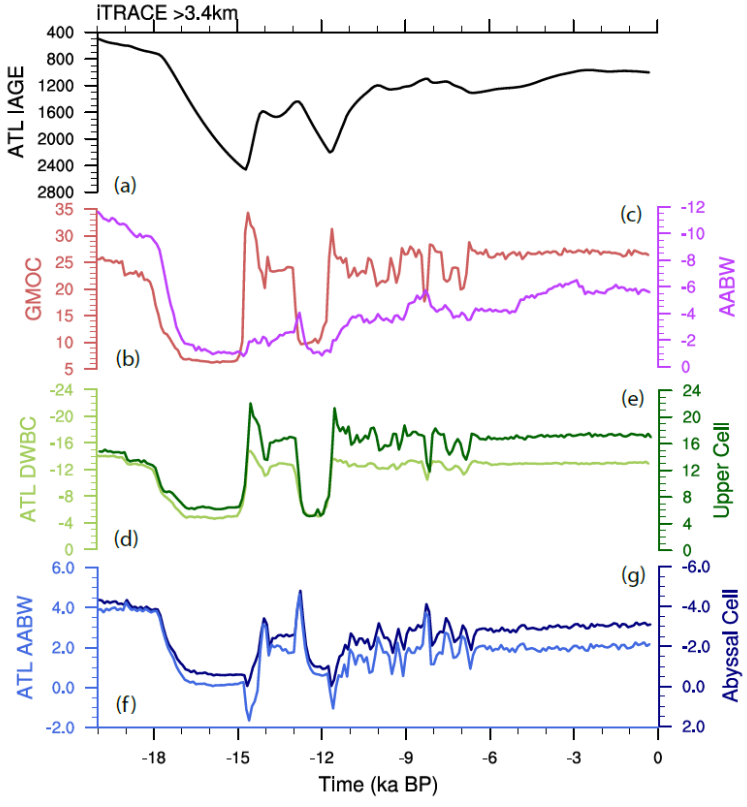

Figure 11 Atlantic deglacial evolutions in the iTRACE: (a) IAGE (black) averaged below 3.4 km, (b) GMOC strength (red), (c) global AABW transport (magenta), (d) Southward DWBC (light green) defined as the southward integrated volume transport within the red box in Figure 11, (e) Upper cell (dark green) defined as the maximum in AMOC between 0.6-3.5 km at 30° S, (f) AABW transport (light blue) defined as $\Psi_{AABW} = -\int_{z=-H}^{z=-3.4km} \int v\, dxdz$ where v is meridional velocity component and H is the bottom seafloor, and (g) abyssal cell (dark blue) defined as the minimum in AMOC below 2.5 km m at 30° S.

More quantitatively, the northward AABW DWBC transport in each basin is calculated from meridional velocity cross section at 30° S, using the same method as in the C-iTRACE. This is due to the approximately flat isopycnals below 3.4 km at 30° S (Fig. 10). The calculated southward DWBC and northward AABW DWBC are validated by the model MOCs, which are defined the same as in the C-iTRACE. The southward DWBC transport and upper cell are mainly differed by the northward return flow in the interior oceans (Fig. 11d-e, Fig. 12d-e). The calculated northward AABW DWBC transport corresponds well with the abyssal cell in each basin (Fig. 11f-g, Fig. 12f-g). Again, in the iTRACE, similar results are obtained such that the correlation between IAGE and northward AABW transport is particularly evident in each basin. Specifically, in the Atlantic, the increasing of IAGE is in alignment with weakening of AAWB transport (Fig. 11a and 11f).

https://doi.org/10.5194/egusphere-2023-2256
Preprint. Discussion started: 9 October 2023

In the deep Indo-Pacific region, the IAGE increases from 825 years at the LGM to 3380 years at 11 ka. After 11 ka, the IAGE remains relatively old around 3400 years, corresponding to the continuous weak AABW transport (Fig. 12a and 12f). Overall, it suggests that weakening AABW transport are the primary cause of the old ventilation ages during deglaciation.

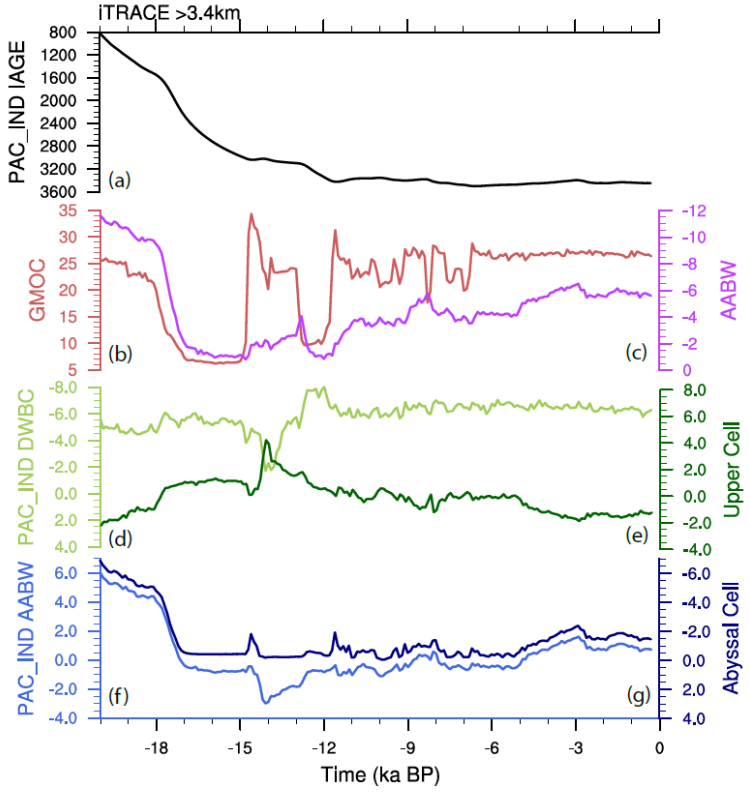

Figure 12 Similar to Fig. 11 but for Indo-Pacific basin.

It should be noted that, in comparison with the bell-shaped temporal pattern observed in the C-iTRACE, the deglacial evolution of IAGE exhibits a distinct temporal behaviour in the iTRACE, with the global deep IAGE increasing from the LGM to the HS1, followed by a continuous presence of old ventilation age until the PD (Fig. 9a). A similar pattern is also seen for the Pacific mean (Fig. 9b). Nevertheless, this distinct deglacial evolution of IAGE is coupled with the transport evolution of AABW (Fig. 9c). A strong AABW transport is simulated at the LGM, followed by a significant reduction during the HS1 and small variability during the Bølling-Allerød warming (BA, 14.7-12.9 ka) and YD. After the Holocene, the AABW transport slowly recovers to its present-day value, which is half (52%) smaller than the LGM value. Consequently, the deep ocean is ventilated at a slower rate due to weaker AABW transport during the Holocene, resulting in a continuous presence of old ventilation age. This is obviously different from C-iTRACE. In the C-iTRACE, the AABW transport at the PD is only 20% smaller than that at the LGM. This in turn results in a slightly older ventilation age at the PD relative to the LGM in the C-iTRACE. Furthermore, the export pathways of AABW from the Southern Ocean into each basin in the iTRACE is somewhat distinct from C-iTRACE results. The major difference between the two simulations lies in

https://doi.org/10.5194/egusphere-2023-2256
Preprint. Discussion started: 9 October 2023

the main export route in the Atlantic. In the iTRACE, AABW tends to flow northward into the Atlantic along the west of the Mid Atlantic Ridge in the Atlantic Ocean (Fig. 13a); along the southwest Pacific basin (Fig. 13b); and along the eastern Indian Ocean basin (Fig. 13c). Nonetheless, the correlation between deep ocean ventilation age and AABW intensity are clearly robust in both simulations.

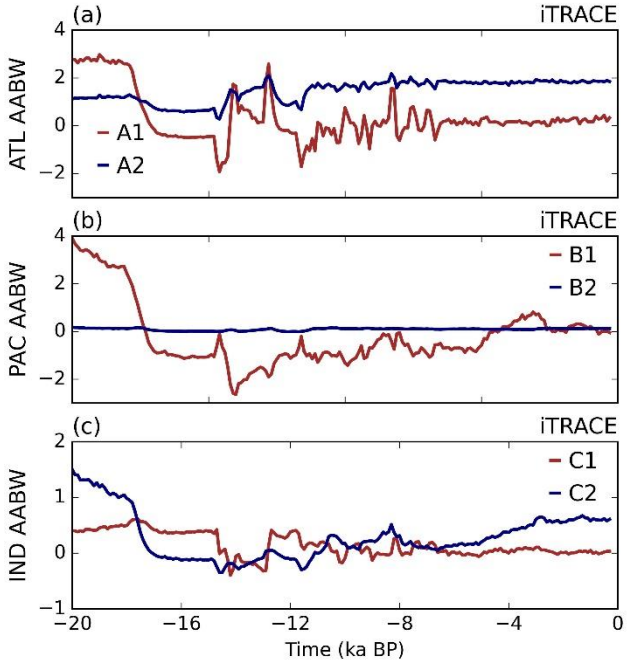

Figure 13 Similar to Fig. 8 but in the iTRACE.

5 Summary

In this study, we have assessed mechanisms of global ventilation age changes during the last deglaciation using the ideal age tracer in two deglacial simulations, C-iTRACE and iTRACE. Results from both simulations suggest that, in contrast to the radiocarbon ventilation ages showing poorly ventilated glacial deep waters, the true ventilation age (IAGE) exhibits an overall modestly younger water age during the LGM relative to the PD, because of the faster overturning of AABW in the simulations. This is also inferred from the new approach of estimated deep ocean water age using radiocarbon age by considering multiple water mass contributions (Fig. 1). This implies that radiocarbon reconstructions are likely biased and may fail to reproduce the true deep ocean ventilation age at the LGM. More importantly, the important role of AABW transport in shaping the global true oceanic ventilation age during deglaciation are confirmed robustly across two transient simulations. The oldest water always occurs around in the deep Pacific, dominating global ocean ventilation age. And the increase of deglacial global deep ocean ventilation age is highly correlated with the reduced transport of the AABW

https://doi.org/10.5194/egusphere-2023-2256
Preprint. Discussion started: 9 October 2023

associated with the sea ice and associated buoyancy flux over the Southern Ocean (Ferrari et al., 2014; Jansen, 2017; Jansen et al., 2018; Jansen & Nadeau, 2016; Liu, 2023; Shin et al., 2003; Sun et al., 2018).

However, we must caution that there are some differences between these two simulations. Major difference is the distinct evolution of AABW volume transport, particularly in the Indo-Pacific sector. In the iTRACE, the AABW transport is simulated to be weaker during the Holocene compared to the C-iTRACE, resulting in a continuous presence of old water age from the late HS1 to early Holocene. This continuous old IAGE during the Holocene is consistent with a recent study showing high-precision radiocarbon results from the Southern Ocean and North Atlantic, demonstrating the millennial stability of Holocene overturing circulation (Chen et al., 2023). In this case, results from iTRACE with higher resolution seems to be more realistic, showing that the ventilation age during the LGM can be much younger than the age at the PD. Therefore, studies with independent models are highly desirable to validate our findings, and increased proxy observations would greatly contribute to further constraining the changes in deglacial ventilation age in the ocean reservoir.

Data Availability

The C-iTRACE data used in this study is available through the NCAR/UCAR Digital Asset Services Hub at https://gdex.ucar.edu/dataset/204_ajahn.html (Gu, Liu, Jahn, et al., 2021). The iTRACE data used in the study are publicly available at https://www.earthsystemgrid.org/dataset/ucar.cgd.ccsm4.iTRACE.html.

Author contribution

Lingwei Li: Conceptualization, Formal analysis, Investigation, Methodology, Writing - original draft preparation. **Zhengyu Liu**: Conceptualization, Funding acquisition, Methodology, Writing - review & editing. **Jinbo Du**: Conceptualization, Writing - review & editing. **Lingfeng Wan**: Writing - review & editing. **Jiuyou Lu**: Writing - review & editing

Competing interests

The authors declare that they have no conflict of interest.

Acknowledgments

This project is supported by NSF (OCN1810681) and the Science and Technology Innovation Project of Laoshan Laboratory (LSKJ202203303). The CESM project is supported primarily by the NSF. This material is based on study supported by the National Center for Atmospheric Research, which is a major facility sponsored by the NSF under Cooperative Agreement

https://doi.org/10.5194/egusphere-2023-2256
Preprint. Discussion started: 9 October 2023

no. 1852977. Computing and data storage resources, including the Cheyenne supercomputer doi:10.5065/D6RX99HX), were provided by the Computational and Information Systems Laboratory (CISL) at NCAR.

References

Adkins, J. F., & Boyle, E. A. (1997). Changing atmospheric Δ14C and the record of deep water paleoventilation ages. *Paleoceanography*, *12*(3), 337–344. https://doi.org/10.1029/97PA00379

Adkins, J. F., Mclntyre, K., & Schrag, D. P. (2002). The salinity, temperature, and delta18O of the glacial deep ocean. *Science*, *298*(5599), 1769–1773. https://doi.org/10.1126/science.1076252. PMID: 12459585.

Brady, E., Stevenson, S., Bailey, D., Liu, Z., Noone, D., Nusbaumer, J., Otto-Bliesner, B. L., Tabor, C., Tomas, R., Wong, T., Zhang, J., & Zhu, J. (2019). The Connected Isotopic Water Cycle in the Community Earth System Model Version 1. *Journal of Advances in Modeling Earth Systems*, *11*(8), 2547–2566. https://doi.org/10.1029/2019MS001663

Burke, A., & Robinson, L. F. (2012). The Southern Ocean's Role in Carbon Exchange During the Last Deglaciation. *Science*, *335*(6068), 557–561. https://doi.org/10.1126/science.1208163

Chen, T., Robinson, L. F., Burke, A., Southon, J., Spooner, P., Morris, P. J., & Ng, H. C. (2015). Synchronous centennial abrupt events in the ocean and atmosphere during the last deglaciation. *Science*, *349*(6255), 1537–1541. https://doi.org/10.1126/science.aac6159

Chen, T., Robinson, L. F., Li, T., Burke, A., Zhang, X., Stewart, J. A., White, N. J., & Knowles, T. D. J. (2023). Radiocarbon evidence for the stability of polar ocean overturning during the Holocene. *Nature Geoscience*, *16*(7), 631–636. https://doi.org/10.1038/s41561-023-01214-2

Danabasoglu, G., Bates, S. C., Briegleb, B. P., Jayne, S. R., Jochum, M., Large, W. G., Peacock, S., & Yeager, S. G. (2012). The CCSM4 Ocean Component. *Journal of Climate*, *25*(5), 1361–1389. https://doi.org/10.1175/JCLI-D-11-00091.1

Ferrari, R., Jansen, M. F., Adkins, J. F., Burke, A., Stewart, A. L., & Thompson, A. F. (2014). Antarctic sea ice control on ocean circulation in present and glacial climates. *Proceedings of the National Academy of Sciences*, *111*(24), 8753–8758. https://doi.org/10.1073/pnas.1323922111

https://doi.org/10.5194/egusphere-2023-2256
Preprint. Discussion started: 9 October 2023

Gu, S., & Liu, Z. (2017). 231Pa and 230Th in the ocean model of the Community Earth System Model (CESM1.3). *Geoscientific Model Development*, *10*(12), 4723–4742. https://doi.org/10.5194/gmd-10-4723-2017

Gu, S., Liu, Z., Jahn, A., Rempfer, J., Zhang, J., & Joos, F. (2019). Modeling Neodymium Isotopes in the Ocean Component of the Community Earth System Model (CESM1). *Journal of Advances in Modeling Earth Systems*, *11*(3), 624–640. https://doi.org/10.1029/2018MS001538

Gu, S., Liu, Z., Jahn, A., & Zanowski, H. (2021). *C-iTRACE* (1.0) [dataset]. UCAR/NCAR: DASH Repository. https://doi.org/10.5065/hanq-bn92

Gu, S., Liu, Z., Lynch-Stieglitz, J., Jahn, A., Zhang, J., Lindsay, K., & Wu, L. (2019). Assessing the Ability of Zonal δ18O Contrast in Benthic Foraminifera to Reconstruct Deglacial Evolution of Atlantic Meridional Overturning Circulation. *Paleoceanography and Paleoclimatology*, 2019PA003564. https://doi.org/10.1029/2019PA003564

Gu, S., Liu, Z., Oppo, D. W., Lynch-Stieglitz, J., Jahn, A., Zhang, J., Lindsay, K., & Wu, L. (2021). Remineralization dominating the δ13C decrease in the mid-depth Atlantic during the last deglaciation. *Earth and Planetary Science Letters*, *571*, 117106. https://doi.org/10.1016/j.epsl.2021.117106

Gu, S., Liu, Z., Oppo, D. W., Lynch-Stieglitz, J., Jahn, A., Zhang, J., & Wu, L. (2020). Assessing the potential capability of reconstructing glacial Atlantic water masses and AMOC using multiple proxies in CESM. *Earth and Planetary Science Letters*, *541*, 116294. https://doi.org/10.1016/j.epsl.2020.116294

He, C., Liu, Z., Otto-Bliesner, B. L., Brady, E. C., Zhu, C., Tomas, R., Buizert, C., & Severinghaus, J. P. (2021a). Abrupt Heinrich Stadial 1 cooling missing in Greenland oxygen isotopes. *Science Advances*, *7*(25), eabh1007. https://doi.org/10.1126/sciadv.abh1007

He, C., Liu, Z., Otto-Bliesner, B. L., Brady, E. C., Zhu, C., Tomas, R., Clark, P. U., Zhu, J., Jahn, A., Gu, S., Zhang, J., Nusbaumer, J., Noone, D., Cheng, H., Wang, Y., Yan, M., & Bao, Y. (2021b). Hydroclimate footprint of pan-Asian monsoon water isotope during the last deglaciation. *Science Advances*, *7*(4), eabe2611. https://doi.org/10.1126/sciadv.abe2611

https://doi.org/10.5194/egusphere-2023-2256
Preprint. Discussion started: 9 October 2023

Hesse, T., Butzin, M., Bickert, T., & Lohmann, G. (2011). A model-data comparison of δ^{13}C in the glacial Atlantic Ocean: DELTA C-13 IN THE GLACIAL ATLANTIC. *Paleoceanography*, *26*(3), n/a-n/a. https://doi.org/10.1029/2010PA002085

Hurrell, J. W., Holland, M. M., Gent, P. R., Ghan, S., Kay, J. E., & Kushner, P. J. (2013). The Community Earth System Model: A Framework for Collaborative Research. *Bulletin of the American Meteorological Society*, *94*(9), 1339–1360. https://doi.org/10.1175/BAMS-D-12-00121.1

Jahn, A., Lindsay, K., Giraud, X., Gruber, N., Otto-Bliesner, B. L., Liu, Z., & Brady, E. C. (2015). Carbon isotopes in the ocean model of the Community Earth System Model (CESM1). *Geoscientific Model Development*, *8*(8), 2419–2434. https://doi.org/10.5194/gmd-8-2419-2015

Jansen, M. F. (2017). Glacial ocean circulation and stratification explained by reduced atmospheric temperature. *Proceedings of the National Academy of Sciences*, *114*(1), 45–50. https://doi.org/10.1073/pnas.1610438113

Jansen, M. F., & Nadeau, L.-P. (2016). The Effect of Southern Ocean Surface Buoyancy Loss on the Deep-Ocean Circulation and Stratification. *Journal of Physical Oceanography*, *46*(11), 3455–3470. https://doi.org/10.1175/JPO-D-16-0084.1

Jansen, M. F., Nadeau, L.-P., & Merlis, T. M. (2018). Transient versus Equilibrium Response of the Ocean's Overturning Circulation to Warming. *Journal of Climate*, *31*(13), 5147–5163. https://doi.org/10.1175/JCLI-D-17-0797.1

Johnson, G. C. (2008). Quantifying Antarctic Bottom Water and North Atlantic Deep Water volumes. *Journal of Geophysical Research: Oceans*, *113*(C5). https://doi.org/10.1029/2007JC004477

Liu, Z. (2023). Evolution of Atlantic Meridional Overturning Circulation since the Last Glaciation: Model simulations and relevance to present and future. *Philosophical Transactions A*, *381*(22022190). https://doi.org/10.1098/rsta.2022.0190.

Liu, Z., Otto-Bliesner, B. L., He, F., Brady, E. C., Tomas, R., Clark, P. U., Carlson, A. E., Lynch-Stieglitz, J., Curry, W., Brook, E., Erickson, D., Jacob, R., Kutzbach, J., & Cheng, J. (2009). Transient Simulation of Last Deglaciation with a New Mechanism for Bølling-Allerød Warming. *Science*, *325*(5938), 310–314. https://doi.org/10.1126/science.1171041

https://doi.org/10.5194/egusphere-2023-2256
Preprint. Discussion started: 9 October 2023

Lund, D. C., Mix, A. C., & Southon, J. (2011). Increased ventilation age of the deep northeast Pacific Ocean during the last deglaciation. *Nature Geoscience*, *4*(11), 771–774. https://doi.org/10.1038/ngeo1272

Marchitto, T. M., Lehman, S. J., Ortiz, J. D., Flückiger, J., & Geen, A. v. (2007). Marine Radiocarbon Evidence for the Mechanism of Deglacial Atmospheric CO2 Rise. *Science*, *316*(5830), 1456–1459. https://doi.org/10.1126/science.1138679

Marshall, J., & Speer, K. (2012). Closure of the meridional overturning circulation through Southern Ocean upwelling. *Nature Geoscience*, *5*(3), 171–180. https://doi.org/10.1038/ngeo1391

Monnin, E., Indermühle, A., Dällenbach, A., Flückiger, J., Stauffer, B., Stocker, T. F., Raynaud, D., & Barnola, J.-M. (2001). Atmospheric CO2 Concentrations over the Last Glacial Termination. *Science*, *291*(5501), 112–114. https://doi.org/10.1126/science.291.5501.112

Negre, C., Zahn, R., Thomas, A. L., Masqué, P., Henderson, G. M., Martínez-Méndez, G., Hall, I. R., & Mas, J. L. (2010). Reversed flow of Atlantic deep water during the Last Glacial Maximum. *Nature*, *468*(7320), Article 7320. https://doi.org/10.1038/nature09508

Okazaki, Y., Timmermann, A., Menviel, L., Harada, N., Abe-Ouchi, A., Chikamoto, M. O., Mouchet, A., & Asahi, H. (2010). Deepwater Formation in the North Pacific During the Last Glacial Termination. *Science*, *329*(5988), 200–204. https://doi.org/10.1126/science.1190612

Purkey, S. G., Smethie, W. M., Gebbie, G., Gordon, A. L., Sonnerup, R. E., Warner, M. J., & Bullister, J. L. (2018). A Synoptic View of the Ventilation and Circulation of Antarctic Bottom Water from Chlorofluorocarbons and Natural Tracers. *Annual Review of Marine Science*, *10*(1), 503–527. https://doi.org/10.1146/annurev-marine-121916-063414

Rafter, P. A., Gray, W. R., Hines, S. K. V., Burke, A., Costa, K. M., Gottschalk, J., Hain, M. P., Rae, J. W. B., Southon, J. R., Walczak, M. H., Yu, J., Adkins, J. F., & DeVries, T. (2022). Global reorganization of deep-sea circulation and carbon storage after the last ice age. *Science Advances*, *8*(46), eabq5434. https://doi.org/10.1126/sciadv.abq5434

https://doi.org/10.5194/egusphere-2023-2256
Preprint. Discussion started: 9 October 2023

Schmitt, J., Schneider, R., Elsig, J., Leuenberger, D., Lourantou, A., Chappellaz, J., Köhler, P., Joos, F., Stocker, T. F., Leuenberger, M., & Fischer, H. (2012). Carbon Isotope Constraints on the Deglacial CO_2 Rise from Ice Cores. *Science*, *336*(6082), 711–714. https://doi.org/10.1126/science.1217161

Schmittner, A. (2003). Southern Ocean sea ice and radiocarbon ages of glacial bottom waters. *Earth and Planetary Science Letters*, *213*(1–2), 53–62. https://doi.org/10.1016/S0012-821X(03)00291-7

Shin, S.-I., Liu, Z., Otto-Bliesner, B. L., Kutzbach, J. E., & Vavrus, S. J. (2003). Southern Ocean sea-ice control of the glacial North Atlantic thermohaline circulation: GLACIAL THERMOHALINE CIRCULATION. *Geophysical Research Letters*, *30*(2). https://doi.org/10.1029/2002GL015513

Sigman, D. M., & Boyle, E. A. (2000). Glacial/interglacial variations in atmospheric carbon dioxide. *Nature*, *407*(6806), 859–869. https://doi.org/10.1038/35038000

Sigman, D. M., Hain, M. P., & Haug, G. H. (2010). The polar ocean and glacial cycles in atmospheric CO2 concentration. *Nature*, *466*(7302), 47–55. https://doi.org/10.1038/nature09149

Skinner, L. C., Fallon, S., Waelbroeck, C., Michel, E., & Barker, S. (2010). Ventilation of the Deep Southern Ocean and Deglacial CO2 Rise. *Science*, *328*(5982), 1147–1151. https://doi.org/10.1126/science.1183627

Skinner, L. C., McCave, I. N., Carter, L., Fallon, S., Scrivner, A. E., & Primeau, F. (2015). Reduced ventilation and enhanced magnitude of the deep Pacific carbon pool during the last glacial period. *Earth and Planetary Science Letters*, *411*, 45–52. https://doi.org/10.1016/j.epsl.2014.11.024

Skinner, L. C., Muschitiello, F., & Scrivner, A. E. (2019). Marine Reservoir Age Variability Over the Last Deglaciation: Implications for Marine CarbonCycling and Prospects for Regional Radiocarbon Calibrations. *Paleoceanography and Paleoclimatology*, *34*(11), 1807–1815. https://doi.org/10.1029/2019PA003667

Skinner, L. C., Primeau, F., Freeman, E., de la Fuente, M., Goodwin, P. A., Gottschalk, J., Huang, E., McCave, I. N., Noble, T. L., & Scrivner, A. E. (2017). Radiocarbon constraints on the glacial ocean circulation and its impact on atmospheric CO2. *Nature Communications*, *8*(1), 16010. https://doi.org/10.1038/ncomms16010

Sun, S., Eisenman, I., & Stewart, A. L. (2018). Does Southern Ocean Surface Forcing Shape the Global Ocean Overturning Circulation? *Geophysical Research Letters*, *45*(5), 2413–2423. https://doi.org/10.1002/2017GL076437

https://doi.org/10.5194/egusphere-2023-2256
Preprint. Discussion started: 9 October 2023

Talley, L. D. (2013). Closure of the Global Overturning Circulation Through the Indian, Pacific, and Southern Oceans: Schematics and Transports. *Oceanography*, *26*(1), 80–97. https://doi.org/10.5670/oceanog.2013.07

Toggweiler, J. R. (1999). Variation of atmospheric CO2 by ventilation of the ocean's deepest water. *Paleoceanography*, *14*(5), 571–588. https://doi.org/10.1029/1999PA900033

Zanowski, H., Jahn, A., Gu, S., Liu, Z., & Marchitto, T. M. (2022). Decomposition of Deglacial Pacific Radiocarbon Age Controls Using an Isotope-Enabled Ocean Model. *Paleoceanography and Paleoclimatology*, *37*(8). https://doi.org/10.1029/2021PA004363

Zhang, J., Liu, Z., Brady, E. C., Oppo, D. W., Clark, P. U., Jahn, A., Marcott, S. A., & Lindsay, K. (2017). Asynchronous warming and δ18O evolution of deep Atlantic water masses during the last deglaciation. *Proceedings of the National Academy of Sciences*, *114*(42), 11075–11080. https://doi.org/10.1073/pnas.1704512114